Available online at www.sciencedirect.com
SCIENCE DIRECT®
Scripta Materialia 50 (2004) 1445–1449
Scripta MATERIALIA
www.actamat-journals.com

Quantitative measurement of deformation-induced martensite in 304 stainless steel by X-ray diffraction

Amar K. De [a], David C. Murdock [b], Martin C. Mataya [c], John G. Speer [a], David K. Matlock [a,*]

[a] *Department of Metallurgy and Materials Engineering, Advanced Steel Processing and Products Research Center, Colorado School of Mines, 1500 Illinois Street, Golden, CO 80401, USA*
[b] *Emerson Process Management, Micro Motion Inc., Boulder, CO 80301, USA*
[c] *Los Alamos National Laboratory, Los Alamos, NM 87545, USA*

Received 21 October 2003; received in revised form 10 February 2004; accepted 10 March 2004

Abstract

A single X-ray diffraction scan is effectively used for identifying and evaluating deformation-induced transformation in 304 austenitic stainless steel. Variations in grain size influence surface constraint and hence the through-thickness transformation response. The initial stage of transformation in this steel is most likely dominated by ε–martensite formation.

Keywords: X-ray diffraction; Stainless steel; Martensitic phase transformation; Shear bands; Stacking faults

1. Introduction

Deformation-induced martensitic transformation in 304 austenitic stainless steels has been reported to give rise to both α′ and ε–martensites during straining at sub-zero temperatures [1–5]. Observations with a high voltage electron microscope (HVEM) have revealed that ε–martensite forms from randomly spaced overlapping stacking faults created during deformation at low temperatures and α′-martensite forms at dislocation pile-ups on closely spaced slip planes, i.e., at shear band intersections [6–8]. The low stacking fault energy (SFE) in 304 austenitic stainless steel makes it amenable to these transformation mechanisms by giving rise to planar faults and dislocation pile-ups [9–12]. The early transformation stage during low temperature deformation is governed by a rather competitive nucleation and growth process of either martensite phase and the type of transformation product that forms largely dictates the strain hardening behavior of the steel [13]. In order that the transformation sequence and thereby the mechanical behavior may be understood better, it is imperative that the type of martensite that forms be precisely characterized.

Quantitative assessment of martensitic transformations in 304 stainless steels have typically been carried out either by the use of magnetic methods or by combined use of X-ray diffraction (XRD) (for austenite) and magnetic saturation methods (for magnetic α′-martensite). The amount of ε–martensite is typically calculated as the difference, $[1 - (V_{\alpha'} + V_{\gamma})]$, where $V_{\alpha'}$ and V_{γ} are the volume fractions of α′-martensite and austenite respectively. This indirect procedure potentially leads to erroneous volume fraction measurements of ε–martensite as two different measurement techniques are required. Moreover, XRD measurements may be erroneous when ignoring hcp-reflections in measurements of the amount of austenite.

It has been demonstrated earlier [4,5] and also in the present study, that ε–martensite appears as a hcp phase with almost all the important hcp reflections in the XRD profile. It is therefore possible to quantitatively assess the phase fractions formed during transformation through simultaneous X-ray diffraction line profile analysis of the fcc, bcc and hcp reflections using a direct comparison method. In this paper, a technique that enables simultaneous measurement of all the phases from a single XRD scan is presented, and its effectiveness in

* Corresponding author. Tel.: +1-3032733775; fax: +1-3032733016.
E-mail address: dmatlock@mines.edu (D.K. Matlock).

1359-6462/$ - see front matter
doi:10.1016/j.scriptamat.2004.03.011

identifying some of the interesting transformation behavior that defines the flow characteristics of this steel is illustrated.

2. Quantitative estimation of phase fractions

The quantitative estimation of phases by X-ray diffraction is based on the principle that the total integrated intensity of all diffraction peaks for each phase in a mixture is proportional to the volume fraction of that phase. If the grains of each phase are randomly oriented, the integrated intensity 'I' of any diffraction peak from phase 'i' is given by [14],

$$I_i^{hkl} = KR_i^{hkl}V_i/2\mu \tag{1}$$

where,

$$K = \left(\frac{I_0 A\lambda^3}{32\pi r}\right)\left[\left(\frac{\mu_0}{4\pi}\right)\frac{e^4}{m^2}\right] \quad \text{and}$$

$$R_{hkl} = \left(\frac{1}{v^2}\right)\left[|F|^2 p\left(\frac{1+\cos^2 2\theta}{\sin^2\theta\cos\theta}\right)\right](e^{-2M})$$

I_i^{hkl}: integrated intensity for (hkl) plane of i-phase, i: γ, α' or ε, K: the instrument factor; R_i^{hkl}: material scattering factor and depends on θ, interplanar spacing of hkl, composition and the crystal structure of the phase i, V_i: volume fraction of phase i, v: volume of unit cell, F_{hkl}: structure factor for reflecting plane (hkl), p: multiplicity factor, e^{-2M}: temperature factor, λ: the wavelength of incident X-ray beam, μ: linear absorption coefficient, A: cross sectional area of incident X-ray beam, I_0: intensity of the incident beam, r: radius of diffractometer circle, e, m: charge and mass of electron.

Therefore, for a steel containing austenite (γ), bcc-martensite (α') and hcp-martensite (ε), Eq. (1) may be written as,

$$I_\gamma = \frac{KR_\gamma V_\gamma}{2\mu}, \quad I_{\alpha'} = \frac{KR_{\alpha'}V_{\alpha'}}{2\mu} \quad \text{and} \quad I_\varepsilon = \frac{KR_\varepsilon V_\varepsilon}{2\mu}$$

Additionally,

$$V_\gamma + V_{\alpha'} + V_\varepsilon = 1 \tag{2}$$

From the above relations, and knowing that $K/2\mu$ is constant in a given X-ray diffraction scan, the volume fraction of austenite and martensite can be derived for numerous peaks as,

$$V_i = \frac{\frac{1}{n}\sum_{j=1}^{n}\frac{I_i^j}{R_i^j}}{\frac{1}{n}\sum_{j=1}^{n}\frac{I_\gamma^j}{R_\gamma^j} + \frac{1}{n}\sum_{j=1}^{n}\frac{I_{\alpha'}^j}{R_{\alpha'}^j} + \frac{1}{n}\sum_{j=1}^{n}\frac{I_\varepsilon^j}{R_\varepsilon^j}} \tag{3}$$

where $i = \gamma$, α' or ε in this instance and n is the number of peaks examined.

Eq. (3) enables simultaneous calculation of the volume fraction of austenite, α'-martensite and ε-martensite in 304 stainless steel from a single XRD scan by measuring the integrated intensity of each reflecting plane of the respective phases and calculating the parameter R for each phase. For this calculation, the crystal structure of each phase is known and the lattice parameters can be calculated from the peak positions and Bragg reflection angles. It is noted that Eq. (3), simplified by $I_\varepsilon^j = 0$, is equivalent to the most commonly used formulation for measuring retained austenite volume fraction in ferrite/austenite mixtures such as dual-phase (DP) or transformation-induced-plasticity (TRIP) steels [15].

3. Material and sample preparation

The chemical composition of the 304 austenitic stainless steel used in this investigation is given in Table 1. The steel was available in the form of 1 mm thick cold rolled and annealed sheet with an as-received austenite grain size of 8 μm. Additionally, some steel sheets were heat treated at 1100 °C for 30 min. followed by air cooling to produce a coarser grain size, 58 μm to examine the effect of grain size on the measurement technique. Longitudinal tensile specimens with a reduced gauge section 12.7 mm wide by 80 mm in length were prepared. The tensile samples were deformed with a special fixture assembly adapted to a commercial electromechanical tensile testing system [16]. During testing the samples were submersed in an ethanol bath held at −50 °C and strain was measured over a 50 mm gauge length with a submersible extensometer. Samples were strained at 5.2×10^{-4} s^{-1} to pre-set engineering strain levels of 5%, 10%, 15%, 20%, 30% and 40%.

The low temperature bath was magnetically stirred to maintain a homogeneous temperature and also to reduce the adiabatic heating effect during deformation.

Small rectangular specimens were cut from the gauge length of the strained samples for X-ray diffraction analysis using Cu K_α radiation. To assess the effects of surface constraint on the transformation response, diffraction patterns were obtained on samples chemically thinned to remove specific fractions of the sheet thickness. The solution used for surface removal was a mixture of hydrochloric acid, nitric acid and distilled water in 1:1:1 proportion.

Table 1
Chemical composition of the 304 stainless steel (wt.%)

C	Mn	Cr	Ni	Mo	Cu	Si	Nb
0.06	1.54	18.47	8.3	0.30	0.37	0.48	0.027

4. Results and discussion

Fig. 1 shows the volume fraction of α′-martensite and ε–martensite in both fine-grained and coarse-grained specimens strained 30% at −50 °C as a function of distance from the original specimen surface. It is seen that a stable and uniform volume fraction of α′-martensite can be assessed only beyond a quarter thickness depth from the surface. This effect is attributed to compatibility effects of unconstrained surface grains in the larger grain size sample and not to the diffraction technique discussed here. The effect is minimal in fine-grained material. Thus, to evaluate the X-ray diffraction technique discussed here, all data presented below were obtained after chemically removing a quarter of the specimen thickness. Fig. 1 also indicates the ε–martensite fraction as a function of through-thickness position in the specimens and shows that the ε–martensite volume fraction is almost independent of specimen thickness. Since the ε–martensite formation is stress-assisted, it is less influenced by the strain variations in the through-thickness direction.

Fig. 2 shows a typical XRD profile of the 304 stainless steel for the coarse grain sample strained 15% at −50 °C. The diffraction scan was obtained at room temperature using Cu K_α radiation. The individual diffracting planes from the fcc-austenite, hcp-martensite and bcc-martensite can be clearly identified and are labeled in the figure. The presence of $(100)_\varepsilon$, $(101)_\varepsilon$ and $(102)_\varepsilon$ peaks are clearly revealed and indicate the formation of the hexagonal ε–martensite phase during deformation. These peaks are free of interference from the adjoining peaks and the intensities are strong enough to be easily measurable. Additionally, the $(110)_{\alpha'}$, $(200)_{\alpha'}$ and $(211)_{\alpha'}$ peaks also are present characterizing the bcc-martensite. Using the $(220)_\gamma$, $(311)_\gamma$ reflections for austenite, $(200)_{\alpha'}$, $(211)_{\alpha'}$ for α′–martensite and $(101)_\varepsilon$, $(102)_\varepsilon$ for ε–martensite, the volume fraction of each phase was estimated using Eq. (3). Two reflections from each phase were used to quantify phase fractions. Texture measurements in strained 304 stainless steel samples of different grain sizes indicated only weak texturing and correspondingly, the present measurements are expected to be independent of texture effects. However, in the event of extensive texturing of grains, the present methodology may be successfully applied for phase fraction determination through inclusion of additional peak reflections in the derivation.

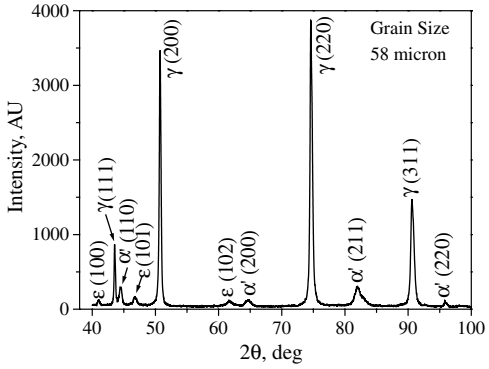

Fig. 2. X-ray diffraction scan using Cu K_α radiation of a 304 SS sample strained 15% at −50 °C showing the presence of ε-hcp, α′-martensite and austenite phases.

Fig. 3 shows the typical microstructure of the coarse grain sample revealing different martensite morphologies formed in the 304 stainless steel after 10% elongation at −50 °C. The parallel ε–martensite plates can be clearly distinguished from the more irregular, rough-edged α′-martensite [2,17]. The α′-martensite appears at the intersections of the shear bands (i.e., ε–platelets) and grows with a similar habit.

Fig. 4 summarizes the volume fraction of austenite, ε- and α′-martensite phases calculated using Eq. (3) as a

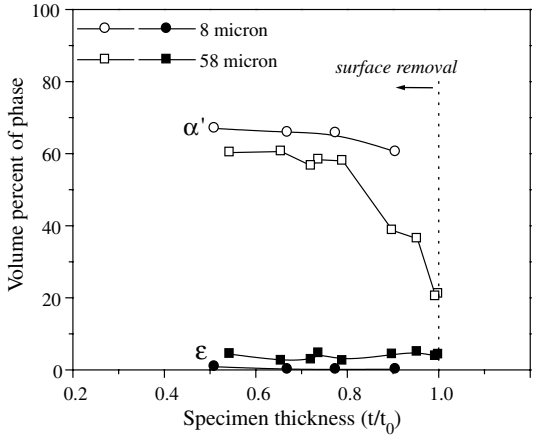

Fig. 1. Grain size effect on phase analysis by X-ray diffraction across the thickness of 304 stainless steel deformed to engineering strain of 30% at −50 °C.

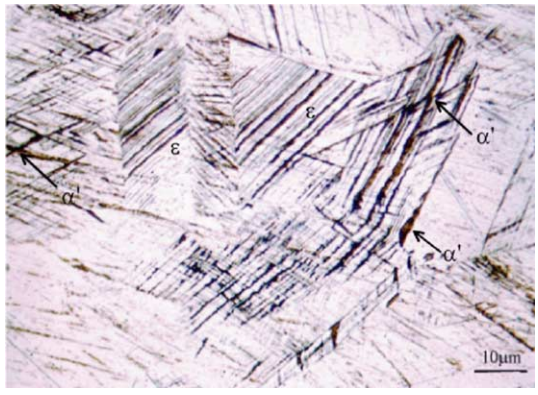

Fig. 3. Microstructure of the coarse-grained 304 austenitic stainless steel sample strained 10% at −50 °C, indicating both the ε–martensite and α′-martensite.The sample was etched in a solution of 10% HCl and 0.25% sodium metabisulfite.

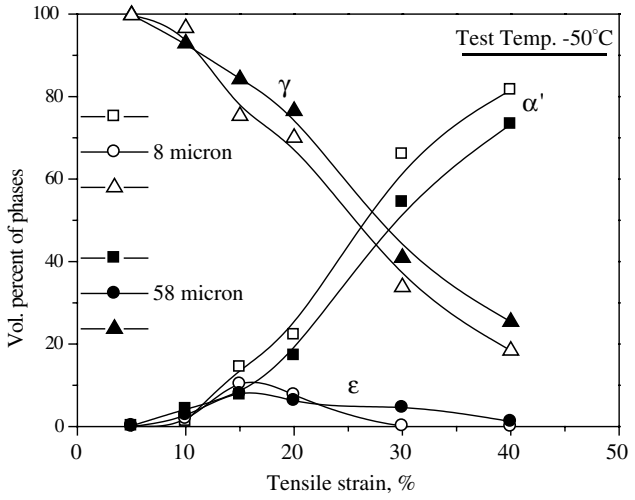

Fig. 4. Variation in martensite and retained austenite phase fractions as a function of strain at −50 °C.

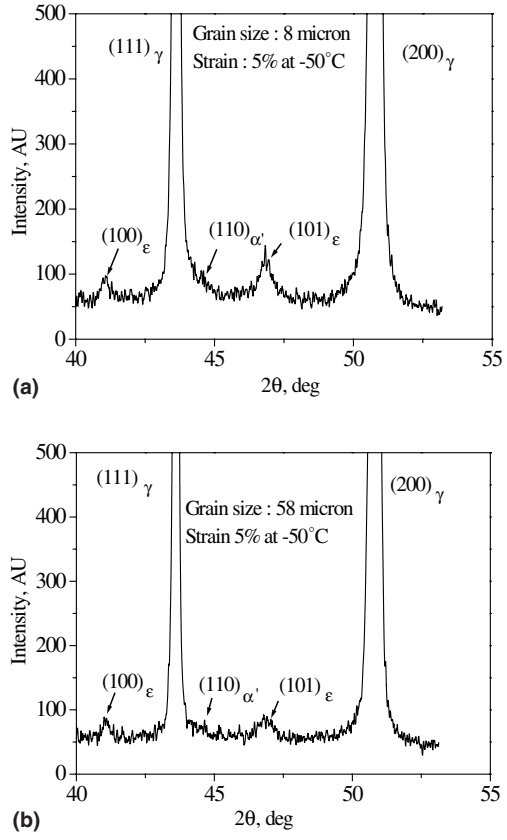

Fig. 5. X-ray diffraction traces of 304 stainless steel for two different grain sizes obtained after 5% straining at −50 °C showing clear reflections from ε-martensite. (a) Grain size: 8 μm, (b) Grain size: 58 μm.

function of deformation strain at −50 °C for two different grain sizes of the steel. The volume fraction of all the phases could be readily measured over the strain range used. The transformation process appeared to require an initial amount of plastic strain in the austenite as both types of martensite were observed to form only after 5% strain. For both grain sizes, the amount of α′-martensite increased with tensile strain and followed a sigmoidal path reaching a saturation volume fraction of approximately 80%. ε–martensite increased in tandem with α′-martensite up to a maximum at 15% strain and decreases thereafter.

Closer examination of the XRD patterns of 5% strained fine and coarse grain samples reveals (Fig. 5) that significant reflections from the ε–martensite phase were observed and the fraction could be measured, while the reflection from α′-martensite was almost absent or immeasurable. Deformation-induced transformation in 304 austenitic stainless steel is apparently initiated by ε–martensite formation followed by α′-martensite. Thus, the initial stages of strain hardening are most likely to be influenced by the ε–martensite formation mechanism.

The results in Fig. 4 also indicate a slight grain size dependency of α′-martensite formation in the 304 steel. The volume fraction of martensite is higher for the fine grain sample, particularly at higher tensile strains. This behavior will be examined in detail in a later publication.

5. Conclusions

The primary aim of the present work was to explore the use of XRD measurements to follow deformation-induced martensite transformation in 304 stainless steel at sub-zero temperature and to characterize the martensitic transformation based on the analysis of a single XRD scan. The proposed methodology demonstrates that the martensite transformation may be effectively characterized in terms of volume fraction of phases formed during deformation through the analysis of a single XRD profile. Grain size influences significantly the surface constraint posed to deformation and hence the transformation, and a uniform bulk measurement is achieved beyond the quarter thickness position in the specimens. This effect is smaller for fine-grained specimens.

XRD analysis revealed that larger amount of ε–martensite forms compared to that of α′-martensite during the initial stages of straining in the 304 steel, and this phenomenon is likely to influence significantly the strain hardening behavior of the steel.

Acknowledgements

The authors acknowledge the support of the Advanced Steel Processing and Products Research Center (ASPPRC), a National Science Foundation Industry/University Cooperative Research Center at Colorado

School of Mines. Support of Amy Streicher, graduate student at ASPPRC, in developing the spreadsheet for calculation of the volume fraction is greatly appreciated.

References

[1] Angel T. JISI 1954;177:165.
[2] Lecroisey F, Pineau A. Metall Trans 1972;3:387.
[3] Cina B. JISI 1954;(August):406.
[4] Mangonon Jr L, Thomas G. Metall Trans 1970;1A:1577.
[5] Mangonon Jr L, Thomas G. Metall Trans 1970;1:1587.
[6] Suzuki T, Kojima H, Suzuki K, Hashimoto T, Ichihara M. Acta Metall 1977;25:1151.
[7] Brooks JW, Loretto MH, Smallman RE. Acta Metall 1979;27:1829.
[8] Brooks JW, Loretto MH, Smallman RE. Acta Metall 1979;27:1839.
[9] Venables JA. J Phys Chem Solids 1964;25:693.
[10] Kelly PM, Nutting J. JISI 1961;March:199.
[11] Yang JH, Wayman CM. Acta Metall Mater 1992;8:2025.
[12] Schramm RE, Reed RP. Metall Trans 1975;6A:1345.
[13] Guntner CJ, Reed RP. Trans ASM 1962;55:399.
[14] Cullity BD, Stock SR. Elements of X-ray diffraction. 3rd ed. New Jersey: Prentice Hall; 2001. p. 351.
[15] ASTM Standard E975. 1984:787.
[16] Peterson SF, Mataya MC, Matlock DK. JOM 1997;(September):54.
[17] Otte HM. Acta Metall 1957;5:614.